The ISME Journal, 2025, **19(1)**, wraf115
https://doi.org/10.1093/ismejo/wraf115
Advance access publication: 2 June 2025
Original Article

Oxygen isotope fractionation during anaerobic ammonium oxidation by the marine representative *Candidatus* Scalindua sp.

Kanae Kobayashi[1,2], Kazuya Nishina[3], Keitaro Fukushima[4,5], Yuji Onishi[4,6], Akiko Makabe[2], Mamoru Oshiki[1], Keisuke Koba[4], Satoshi Okabe[1,*]

[1]Division of Environmental Engineering, Faculty of Engineering, Hokkaido University, Sapporo, Hokkaido 060-8628, Japan
[2]Institute for Extra-cutting-edge Science and Technology Avant-garde Research (X-star), Japan Agency for Marine-Earth Science and Technology (JAMSTEC), Yokosuka 237-0061, Japan
[3]Biogeochemical Cycle Modeling and Analysis Section, Earth System Division, National Institute for Environmental Studies, Onogawa, Tsukuba 305-8506, Japan
[4]Center for Ecological Research, Kyoto University, Otsu, Shiga 520-2113, Japan
[5]Present address: Faculty of Food and Agricultural Sciences, Fukushima University, 1 Kanayagawa, Fukushima, 960-1296, Japan
[6]Present address: Research Institute for Humanity and Nature, 457-4, Kamigamo-Motoyama, Kita-ku, Kyoto, 603-8047, Japan

*Corresponding author. Division of Environmental Engineering, Faculty of Engineering, Hokkaido University, Kita 13 Nishi 8, Kita-ku, Sapporo, Hokkaido 060-8628, Japan. E-mail: sokabe@eng.hokudai.ac.jp

Abstract

Analysing the nitrogen ($^{15}\varepsilon$) and oxygen ($^{18}\varepsilon$) isotope effects of anaerobic ammonium oxidation (anammox) is essential for accurately assessing its potential contribution to fixed-N losses in the ocean, yet the $^{18}\varepsilon$ of anammox remains unexplored. Here, we determined the previously unexplored $^{18}\varepsilon$ of anammox using a highly enriched culture of the marine anammox species "*Ca*. Scalindua sp". Because *Scalindua* significantly accelerated oxygen isotope exchange between NO_2^- and H_2O, we introduced a new rate constant for anammox-mediated oxygen isotope exchange ($k_{eq,\,AMX} = 8.44 \sim 13.56 \times 10^{-2}\ h^{-1}$), which is substantially faster than abiotic oxygen isotope exchange ($k_{eq,\,abio} = 1.13 \times 10^{-2}\ h^{-1}$), into a numerical model to estimate the $^{18}\varepsilon$ during anammox. Based on our experimental results, we successfully determined the $^{18}\varepsilon$ associated with: (1) conversion of NO_2^- to N_2 ($^{18}\varepsilon_{NO2\text{-}\rightarrow N2} = 10.6 \sim 16.1‰$), (2) NO_2^- oxidation to NO_3^- ($^{18}\varepsilon_{NO2\text{-}\rightarrow NO3\text{-}} = -2.9 \sim -11.0‰$, inverse fractionation), (3) incorporation of oxygen from water during NO_2^- oxidation to NO_3^- ($^{18}\varepsilon_{H2O} = 16.4 \sim 19.2‰$). Our study underscores the possibility that unique anammox oxygen isotope signals may be masked due to substantial anammox-mediated oxygen isotope exchange between NO_2^- and H_2O. Therefore, careful consideration is required when utilizing $\delta^{18}O_{NO3\text{-}}$ and $\delta^{18}O_{NO2\text{-}}$ as geochemical markers to assess the potential contribution of anammox to fixed-N losses in the ocean.

Graphical abstract

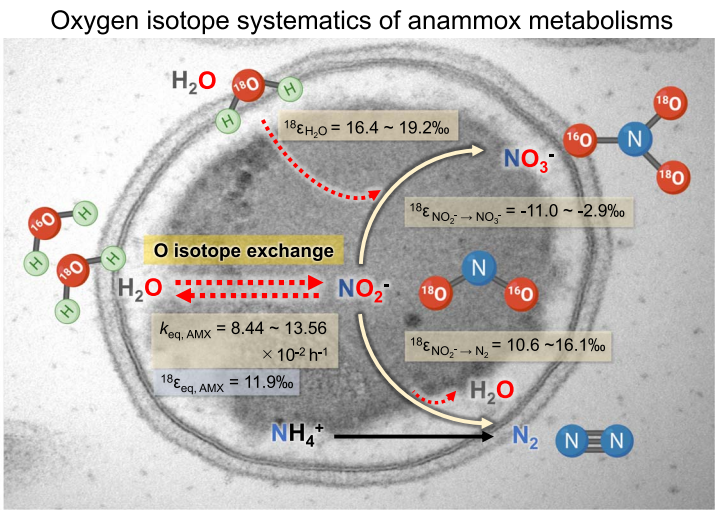

Keywords: anammox; *Scalindua* sp.; kinetic oxygen isotope effect; oxygen isotope exchange between NO_2^- and H_2O

Received: 26 October 2024. **Revised:** 1 April 2025. **Accepted:** 30 May 2025

Introduction

Anaerobic ammonium oxidation (anammox) and denitrification are the two primary sinks of fixed nitrogen in marine ecosystems. Anammox bacteria oxidize NH_4^+ directly to N_2 gas using NO_2^- as the terminal electron acceptor, and simultaneously oxidize NO_2^- to NO_3^- [1], as represented by the following stoichiometric equation [2]:

$$1\mathbf{NH_4^+} + 1.146\mathbf{NO_2^-} + 0.071\mathbf{HCO_3^-} + 0.057\mathbf{H^+} \rightarrow 0.986\mathbf{N_2} + 0.161\mathbf{NO_3^-} + 0.071\mathbf{CH_{1.74}O_{0.31}N_{0.20}} + 2.002\mathbf{H_2O}$$

The significant role of anammox bacteria in nitrogen removal has been documented in oxygen-deficient water columns [3–8] and marine sediments [9–13]. In these ecosystems, the stable isotope ratios of nitrogen ($^{15}N/^{14}N$) and oxygen ($^{18}O/^{16}O$) in reactive nitrogen compounds (e.g. NH_4^+, NO_2^-, and NO_3^-) have been used as geochemical tracers to evaluate nitrogen sources and sinks [14–21] and to determine *in situ* turnover rates [22]. To quantitatively assess the impacts of microbial processes on nitrogen pools, isotope fractionation is measured using the kinetic isotope effect, defined as $\varepsilon\ (‰) = [(k_L / k_H) - 1] \times 1000$, where k_L / k_H represents the ratio of the first-order reaction rate constants between the light (k_L) and heavy (k_H) isotopically substituted substrates. The kinetic nitrogen and oxygen isotope effects ($^{15}\varepsilon$ and $^{18}\varepsilon$) in key microbial processes provide a fundamental basis for interpreting natural abundance nitrogen isotopic distributions in the ocean. The dual isotope effects ($^{15}\varepsilon$ and $^{18}\varepsilon$) associated with anammox metabolism enable a more precise assessment of its contributions to nitrogen loss.

$^{15}\varepsilon$ values for anammox metabolism have been determined for four anammox species; "*Ca*. Kuenenia stuttgartiensis" [23], "*Ca*. Scalindua japonica", "*Ca*. Jettenia caeni", and "*Ca*. Brocadia sinica", all of which were cultured in continuous bioreactors [24]. Additionally, isotope effects have been measured for biomass containing anammox bacteria originating from wastewater treatment plants [25, 26].

Despite its significance, little information is available on the oxygen isotope effects ($^{18}\varepsilon$) of individual anammox reaction pathways. Anammox, denitrification, and nitrification concurrently influence the oxygen isotope composition of nitrite ($\delta^{18}O_{NO2-}$) and nitrate ($\delta^{18}O_{NO3-}$), making the quantification of $^{18}\varepsilon$ associated with individual anammox metabolism essential for estimating its contribution to $\delta^{18}O_{NO2-}$ and $\delta^{18}O_{NO3-}$ in the natural environments. This quantification is very complicated because three reactions influencing the values of $\delta^{18}O_{NO2^-}$ and $\delta^{18}O_{NO3^-}$ (NO_2^- reduction to N_2, NO_2^- oxidation to NO_3^-, and NO_2^- equilibration with H_2O) occur simultaneously during anammox reaction, and the following four associated $^{18}\varepsilon$ must be determined: (i) NO_2^- reduction to N_2 ($^{18}\varepsilon_{NO2- \rightarrow N2}$), (ii) NO_2^- oxidation to NO_3^- ($^{18}\varepsilon_{NO2- \rightarrow NO3-}$), (iii) incorporation of an O atom from H_2O during NO_2^- oxidation to NO_3^- ($^{18}\varepsilon_{H2O}$), and (iv) abiotic and anammox-mediated oxygen isotope exchange between NO_2^- and H_2O ($^{18}\varepsilon_{eq,\ abio}$ and $^{18}\varepsilon_{eq,\ AMX}$) (Fig. 1). To date, only the combined oxygen isotope effects for NO_2^- oxidation to NO_3^- ($^{18}E_{NO2- \rightarrow NO3-} = 2/3\ ^{18}\varepsilon_{NO2- \rightarrow NO3-} + 1/3\ ^{18}\varepsilon_{H2O}$) have been reported for three enrichment cultures of anammox bacteria [24]. Additionally, the oxygen isotope effect during the NO_2^- oxidation to NO_3^- ($^{18}\varepsilon_{NO2- \rightarrow NO3-}$) has been estimated for biomass containing anammox bacteria from a wastewater treatment plant, but lacks high precision [25]. The individual oxygen isotope effects of each anammox reaction pathway ($^{18}\varepsilon_{NO2- \rightarrow N2}$, $^{18}\varepsilon_{NO2- \rightarrow NO3-}$ and $^{18}\varepsilon_{H2O}$) remain entirely unexplored.

To interpret $\delta^{18}O_{NO2-}$ and $\delta^{18}O_{NO3-}$ in environments, it is essential to evaluate oxygen isotope uptake from ambient H_2O and O_2 into NO_2^- and NO_3^- during nitrification as well as abiotic or biologically enhanced oxygen isotope exchange between NO_2^- and H_2O. Oxygen isotope effects resulting from O atom uptake from O_2 or H_2O, along with O isotope exchange between NO_2^- and H_2O during nitrification, have been assessed by $H_2{}^{18}O$ labeling experiments in various systems, including pure culture of ammonia-oxidizing bacteria (AOB) [27] and nitrite-oxidizing bacteria (NOB) [28], an enrichment culture of thermophilic ammonia-oxidizing archaea (AOA) [29], nitrifying cocultures and natural marine assemblages [30], and stream water [31]. Quantifying the influence of the O isotopic composition of water ($\delta^{18}O_{H2O}$) is crucial, as $\delta^{18}O_{NO2-}$ and $\delta^{18}O_{NO3-}$ are strongly affected by both O isotope exchange between NO_2^- and H_2O and O atom uptake from H_2O during nitrification.

Here we quantified the kinetic oxygen isotope effects ($^{18}\varepsilon_{NO2- \rightarrow N2}$, $^{18}\varepsilon_{NO2- \rightarrow NO3-}$ and $^{18}\varepsilon_{H2O}$) as well as the rate constant for anammox-mediated O isotope exchange between NO_2^- and H_2O ($k_{eq,\ AMX}$) associated with anammox metabolism in a marine anammox species "*Ca*. Scalindua sp." [32]. We conducted a series of batch culture experiments with "*Ca*. Scalindua sp." under varying $\delta^{18}O_{H2O}$ medium conditions and determined the kinetic O isotope effects using a newly developed numerical model.

Materials and methods

Experimental design

The objective of this study was to determine the previously unexplored $^{18}\varepsilon$ and O atom exchange between NO_2^- and H_2O associated with anammox metabolism using a highly enriched marine anammox culture of "*Ca*. Scalindua sp.". To achieve this objective, we conducted a series of batch culture experiments with "*Ca*. Scalindua sp." in different $\delta^{18}O_{H2O}$ media and measured the time-dependent dynamics of concentrations and isotope compositions of nitrogen compounds (NH_4^+, NO_2^-, and NO_3^-). We estimated $^{15}\varepsilon$ and $^{18}\varepsilon$ for the respective reaction pathways of anammox metabolism using Markov Chain Monte Carlo (MCMC) method implemented in a newly constructed numerical model.

Enrichment culture of "*Ca*. Scalindua sp."

Free-living planktonic enrichment cultures of a marine anammox bacteria species "*Ca*. Scalindua sp." were cultivated in a 3 L membrane bioreactor (MBR) equipped with a hollow fiber membrane module (pore size 0.1 μm, polyethylene) as previously described (Fig. S15) [33–35]. The inorganic nutrient medium continuously fed into the MBR contained the following: KH_2PO_4 (24.4 mg L^{-1}), $MgSO_4{\cdot}7H_2O$ (99 mg L^{-1}), $CaCl_2$ (86 mg L^{-1}), and 0.5 ml trace element solution I and II [36]. Equimolar amounts of $NH_4(SO_4)_2$ and $NaNO_2$ were added to achieve 10 mmol-N L^{-1}. An artificial sea salt SEALIFE (Marine Tech, Tokyo, Japan) was supplemented into the media to achieve 2.5% salinity. The culture fluid in the MBR was continuously mixed with a magnetic stirrer at 200 rpm and sparged with 95% Ar-5% CO_2 at a flow rate of 10 ml min^{-1}. The pH was not controlled but remained between 7.3 and 7.8. The temperature was maintained at 30°C.

Experiments for nitrogen and oxygen isotope effects during anammox

The enriched anammox bacterial cells were collected from MBRs operated at steady-state and further enriched by Percoll density gradient centrifugation [37]. The ratio of anammox bacteria to total cells (degree of enrichment) in the Percoll-centrifuged

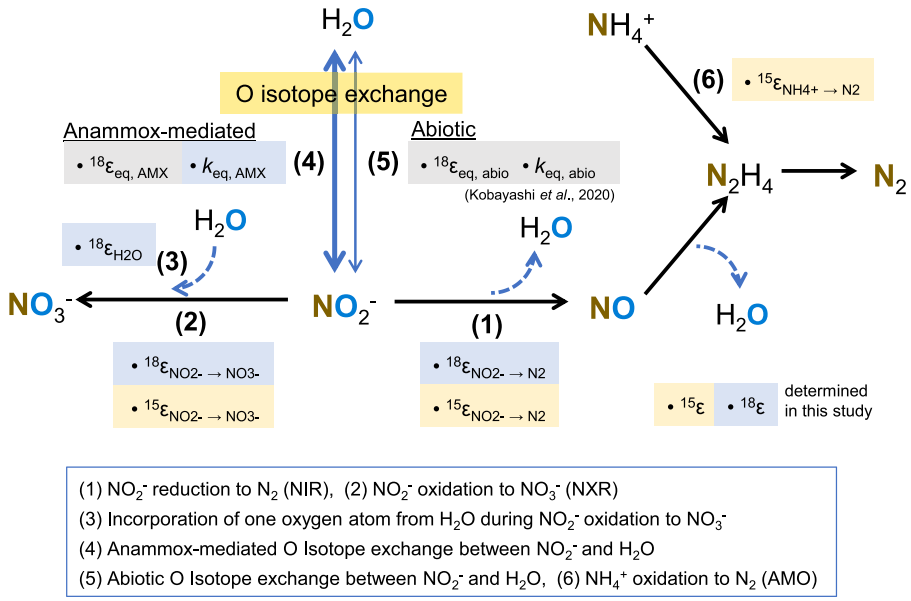

Figure 1. Description of anammox metabolism and associated nitrogen and oxygen isotope effects. $\delta^{18}O_{NO_2^-}$ and $\delta^{18}{}_{NO_3^-}$ are influenced by reaction (1), reaction (2), and the equilibrium between NO_2^- and H_2O, described by reactions (4) and (5). We determined the following three kinetic oxygen isotope effects ($^{18}\varepsilon$); (1) $^{18}\varepsilon_{NO2^-\rightarrow N2}$, (2) $^{18}\varepsilon_{NO2^-\rightarrow NO3^-}$, and (3) $^{18}\varepsilon_{H2O}$, as well as (4) a reaction rate constant ($k_{eq,\ AMX}$) for anammox-mediated oxygen isotope exchange between NO_2^- and H_2O. In our previous study, we determined the equilibrium isotope effect ($^{18}\varepsilon_{eq,\ abio}$) and the reaction rate constant ($k_{eq,\ abio}$) for abiotic oxygen isotope exchange between NO_2^- and H_2O to be 11.9‰ and 1.13×10^{-2} h^{-1}, respectively [45]. We assumed that $^{18}\varepsilon_{eq,\ AMX}$ is identical to $^{18}\varepsilon_{eq,\ abio}$ in the model simulation. Additionally, we determined three nitrogen isotope effects; (1) $^{15}\varepsilon_{NO2^-\rightarrow N2}$, (2) $^{15}\varepsilon_{NO2^-\rightarrow NO3^-}$, and (6) $^{15}\varepsilon_{NH4+-\rightarrow NO2}$ in this study.

culture was >99% based on fluorescent *in situ* hybridization analysis. The highly enriched biomass was washed with mineral medium without NH_4^+ and NO_2^- and resuspended in 0.9 L of the same medium (~10^9 cells ml^{-1}). The biomass was incubated in 1 L glass bottles (Shibata Scientific Technology, Ltd., Saitama, Japan) overnight to completely consume the residual NH_4^+ and NO_2^-. The media for batch culture experiments were prepared as described above, with the following modification: the $\delta^{18}O$ of the H_2O in the medium was adjusted to four different values ($\delta^{18}O_{H2O} = -12.6$‰ (unlabeled), 25.9‰, 56.7‰, and 110.1‰) by adding $H_2{}^{18}O$ (97% ^{18}O; Aldrich, prod. no. 329878). For each medium $\delta^{18}O_{H2O}$ value, batch culture experiments were conducted in triplicate. The temperature was controlled at 30°C. The batch cultures were flushed with an Ar: CO_2 gas mixture and stirred continuously. The pH was not controlled but remained between 7.2 and 7.9 (Average 7.5). The experiments were initiated by adding $NaNO_2$ (at a final concentration of 2.0 mmol-N L^{-1}) and $(NH_4)_2SO_4$ (at a final concentration of 2.5 mmol L^{-1}). The culture medium was continuously mixed using a magnetic stirrer at 200 rpm. To maintain anoxic conditions, a mixed gas (Ar: CO_2 = 95:5) was purged into the culture medium at a flow rate of 10 m min^{-1}. After adding substrates, a total of 25 to 40 ml of the culture solution was periodically sampled. Time course experiments lasted until the NO_2^- had been completely consumed, which usually took approximately from 5 to 7 hours. All samples were immediately filtered using a 0.2-μm cellulose acetate filter (25CS020AN, Advantec, Tokyo, Japan). The pH was measured using 0.5 ml of the sample solution with a pH meter (pH meter B-712, Horiba, Ltd., Kyoto, Japan).

After filtration, sample solutions were immediately adjusted to pH 2 by adding 1 M H_2SO_4 solution and then stored at −20°C until analysis for nitrogen isotope ratios of NH_4^+ to prevent NH_4^+ from volatilizing. To analyse $\delta^{15}N_{NO2^-}$ and $\delta^{18}O_{NO2^-}$, sample solutions were immediately adjusted to pH 12 by adding 2 M low-N-blank NaOH solution after filtration and stored at −20°C until analysis to prevent oxygen isotope exchange between NO_2^- and H_2O during sample storage [38]. To analyse $\delta^{15}N_{NO3^-}$ and $\delta^{18}O_{NO3^-}$, any remaining NO_2^- in the sample solution was immediately removed by adding sulphamic acid (H_3NSO_3) after filtration, as NO_2^- interferes with NO_3^- isotope analysis [39]. The concentration of NO_2^- was measured using the naphthylethylenediamine method [40] to confirm complete removal of NO_2^-. The samples were then stored at −20°C until analysis.

Experiments for nitrogen isotope exchange between NO_2^- and NO_3^-

To investigate N isotope exchange between NO_2^- and NO_3^-, batch culture experiments were conducted by adding 2 ml of 1 M $(NH_4)_2SO_4$ solution, 2 ml of 0.75 M ACROS-NO_2^- solution with a low $\delta^{15}N$ value ($\delta^{15}N_{NO2^-} = -35.5$‰), and 8 ml of 5 mM USGS32 (NO_3^-) solution with a high $\delta^{15}N$ value ($\delta^{15}N_{NO3^-} = 180.0$‰) to 800 ml culture medium. This experiment could only be performed once due to limited quantities of ACROS-NO_2^- and USGS32 (NO_3^-) solutions. The final concentrations of NH_4^+, NO_2^-, and NO_3^- were 2.5, 1.88, and 0.05 mM, respectively. Water with a $\delta^{18}O$ of −12.6‰ was used as the medium. Other experimental procedures were the same as described above. In this experiment, the initial $\delta^{15}N$ difference between NO_2^- and NO_3^- was set large (−215.5‰) to facilitate observation of rapid changes in $\delta^{15}N_{NO2-}$ and $\delta^{15}N_{NO3^-}$ when N isotope exchange occurs during the anammox reaction.

Chemical analyses

On the day of sampling, the following concentrations were analysed using 1.0 ml sample filtrate. The concentration of NH_4^+ was measured by the indophenol blue method [40] using a multi-label plate reader (ARVO MX 1420-01 J; PerkinElmer; Waltham, MA, USA). The NO_2^- concentration was measured by the naphthylethylenediamine method [40]. The concentration of NO_3^- was measured using ion chromatographs (IC-2010, TOSOH; Tokyo, Japan) equipped with a TSKgel IC-Anion HS column (TOSOH; Tokyo, Japan).

Isotopic analyses

NH_4^+ nitrogen isotope analyses were performed using the ammonium diffusion method [41, 42] and subsequently measured by EA-IRMS (Flash EA1112, ConFlo IV interface, Delta plus Advantage; ThremoFinnigan). International and internal NH_4^+ isotopic standards, USGS25 ($\delta^{15}N = -30.41‰$), USGS26 ($\delta^{15}N = 53.75‰$), and IAEA-N-2 ($\delta^{15}N = 20.3‰$), were used for calibration. The one-sigma standard deviations of $\delta^{15}N_{NH_4^+}$ measurements of standards were ± 0.3‰.

NO_2^- nitrogen and oxygen isotope ratios were measured by chemically converting NO_2^- to nitrous oxide (N_2O) using the azide method [43]. All samples were adjusted to the same pH (pH = 12) and salinity (2.5% NaCl). The NO_2^- standard solution had the same pH, salinity, solution volume and $\delta^{18}O_{H2O}$ values as the batch of samples to account for any effects from pH-dependent incorporation of water O atoms into N_2O during its generation. Due to the high sample pH (pH = 12), the azide buffer was modified by increasing the acetic acid concentration to 7.84 M [44] and the sodium azide concentration to 4 M [45]. The sample and standard solutions were buffered at pH 4.4 during the reaction. The N_2O was then analysed in duplicate using a purge-and-trap, gas chromatography isotope ratio mass spectrometry (PT-GC-IRMS). The corrected $\delta^{15}N$ and $\delta^{18}O$ values of the sample N_2O converted from NO_2^- were calibrated against in-house NO_2^- standards; JAM 1 ($\delta^{15}N = -2.5‰$, $\delta^{18}O = 91.7‰$), JAM 2 ($\delta^{15}N = 1.8‰$, $\delta^{18}O = 9.9‰$), JAM 3 ($\delta^{15}N = -26.4‰$, $\delta^{18}O = 39.4‰$), and JAM 4 ($\delta^{15}N = -1.5‰$, $\delta^{18}O = -15.2‰$) [45]. Each reference solution was analysed three times, and triplicate analyses generally yielded precisions of ±0.2‰ for $\delta^{15}N_{NO2-}$ and ± 0.3‰ for $\delta^{18}O_{NO2-}$. The details of sample preparation and measurement are described in our previous publication [45].

NO_3^- nitrogen and oxygen isotope ratios were measured by microbial conversion of NO_3^- to N_2O using the denitrifier method [46, 47]. All samples were exactly adjusted to the same pH and salinity. The NO_3^- standard solutions were prepared with the same pH, salinity and $\delta^{18}O_{H2O}$ value as the batch of samples to be analysed. N_2O was analysed in triplicate using PT-GC-IRMS. The corrected $\delta^{15}N$ and $\delta^{18}O$ values of the sample N_2O converted from NO_3^- were calibrated against international NO_3^- isotopic standards: IAEAN3 ($\delta^{15}N = 4.7‰$, $\delta^{18}O = 25.6‰$), USGS32 ($\delta^{15}N = 180‰$, $\delta^{18}O = 25.7‰$), USGS34 ($\delta^{15}N = -1.8‰$, $\delta^{18}O = -27.9‰$), and USGS35 ($\delta^{18}O = 57.5‰$) [48]. Triplicate analyses generally yielded precisions of ±0.2‰ for $\delta^{15}N_{NO3-}$ and ± 0.5‰ for $\delta^{18}O_{NO3-}$. The details of sample preparation and measurement are described in our previous publication [45].

The $\delta^{18}O_{H2O}$ was measured by equilibration with NO_2^- and subsequent conversion of NO_2^- to N_2O using a modified azide method [49] with 0.5 ml of the samples and standards. The $\delta^{18}O$ data was calibrated against Greenland Ice Sheet Precipitation (GISP, −24.8‰) and in-house water standards: Alaskan bottled mineral water (−19.0‰) and bottled de-salted seawater (0.2‰) (these $\delta^{18}O$ values were determined by SI Science. Co. Ltd). Samples with high $\delta^{18}O_{H2O}$ were mixed with MillQ water (−12.6‰) to yield measured $\delta^{18}O$ values within the range of the standards (i.e. between −24.8‰ and 0.2‰), calculated according to the mixing ratio. Triplicate analyses yielded a precision of 0.20‰ for $\delta^{18}O_{H2O}$.

Calculation of isotopic effects with a numerical model

To estimate N and O isotope effects ($^{15}\varepsilon$ and $^{18}\varepsilon$) for the individual reaction pathways of anammox metabolism (Fig. 1), we developed and modified an ordinary differential equation model as described by Kotajima et al. (2020) [25] and Granger and Wankel (2016) [50] (see Supplemental Materials for details). The basic concept of our model involves taking mass balance of isotope pools (^{14}N, ^{15}N, ^{16}O, and ^{18}O) of NH_4^+, NO_2^-, and NO_3^-. The changes of each pool are expressed using differential equations. To infer each parameter on the N and O isotope effects, the differential equations were solved using the R package FME [51]. All simulations were run using this package, which provides solutions for differential equations with integration algorithms and inverse modeling using the Markov-Chain Monte-Carlo technique. Our model script in R language is available at ZENODO (the code is available at https://zenodo.org/records/15015868).

Because the anammox reaction was assumed to be a zero-order reaction in this model simulation, data points during the initial lag or low active phase were excluded for parameter estimations. The estimation range of each parameter related to N isotope effects was set as follows: $(0 < {}^{15}\varepsilon_{NH4+\rightarrow N2} < 60,\ 0 < {}^{15}\varepsilon_{NO2-\rightarrow N2} < 60,$ and $-60 < {}^{15}\varepsilon_{NO2-\rightarrow NO3-} < 0)$, based on observed data sets and the reported $^{15}\varepsilon$ values of anammox bacteria (Table S4) [23–25]. The MCMC were run for 100 000 iterations after a burn-in period of 50 000 iterations, and the posterior samples were obtained on the remaining iterations. We set the thinning rate was 5. The mean and standard deviation of isotope effect were derived by the overall posteriors consisted with the three independent replication. For the O isotope effects ($^{18}\varepsilon$), uniform probabilities were used for each parameter, set as follows: $(5 < {}^{18}\varepsilon_{NO2-\rightarrow N2} < 20,\quad -15 < {}^{18}\varepsilon_{NO2-\rightarrow NO3-} < 0,\quad 10 < {}^{18}\varepsilon_{H2O} < 25)$ (Table S5). These priors were based on observed data sets and reported $^{18}\varepsilon$ values catalyzed by the same enzymes [28, 30, 31, 52]. The sampling number for the MCMC was also set to 100 000. Details of the model, calculation method and fitting results were described in the Supplementary Materials. To evaluate the validity of the calculation results from the model simulation, the N isotope effects of NH_4^+ oxidation ($^{15}\varepsilon_{NH4+\rightarrow N2}$), NO_2^- reduction ($^{15}\varepsilon_{NO2-\rightarrow N2}$) and NO_2^- oxidation ($^{15}\varepsilon_{NO2-\rightarrow NO3-}$) were also calculated by using the canonical closed-system Rayleigh isotope fractionation systematics [23].

Results and discussion

Batch culture experiments

Batch culture experiments were performed in triplicate using four waters with different $\delta^{18}O$ values ($\delta^{18}O_{H2O} = -12.6‰$ (unlabeled), 25.9‰, 56.7‰, and 110.1‰). The concentrations of NH_4^+, NO_2^-, and NO_3^-, and isotope ratios of nitrogen and oxygen ($\delta^{15}N = {}^{15}N/{}^{14}N$ and $\delta^{18}O = {}^{18}O/{}^{16}O$) were measured over time during the batch culture. After addition of 2.5 mM of NH_4^+ and 2.0 mM of NO_2^-, both NH_4^+ and NO_2^- were almost immediately consumed linearly with time, and NO_3^- was concomitantly produced at constant rates (Fig. 2 A-D and Figs. S1-S4, A - C), indicating that the anammox reaction exhibited the maximum rates according to Michaelis–Menten kinetics at NO_2^-concentration ranges significantly higher than the half-saturation constants (K_m for $NO_2^- \approx 0.1–1.0\ \mu M$) for "*Ca.* Scalindua sp." [53] (Supplementary materials Eq. S5-S7). In some experiments, short lag times and slightly lower active phases were observed (Fig. S2C, Fig. S3C and Fig. S4A). The average stoichiometric ratios of consumed NO_2^- and consumed NH_4^+ ($\Delta NO_2^-/\Delta NH_4^+$) were 1.38 ± 0.10 (mean ± SD) and produced NO_3^- and consumed NH_4^+ ($\Delta NO_3^-/\Delta NH_4^+$) were 0.33 ± 0.04, respectively. These values were slightly higher than those previously reported [2], but close to the one reported by Brunner et al. (2013) [23]. This may suggest that, in batch cultures, a greater proportion of NO_2^- must be disproportionated to NO_3^- and NO to facilitate NH_4^+ activation [54].

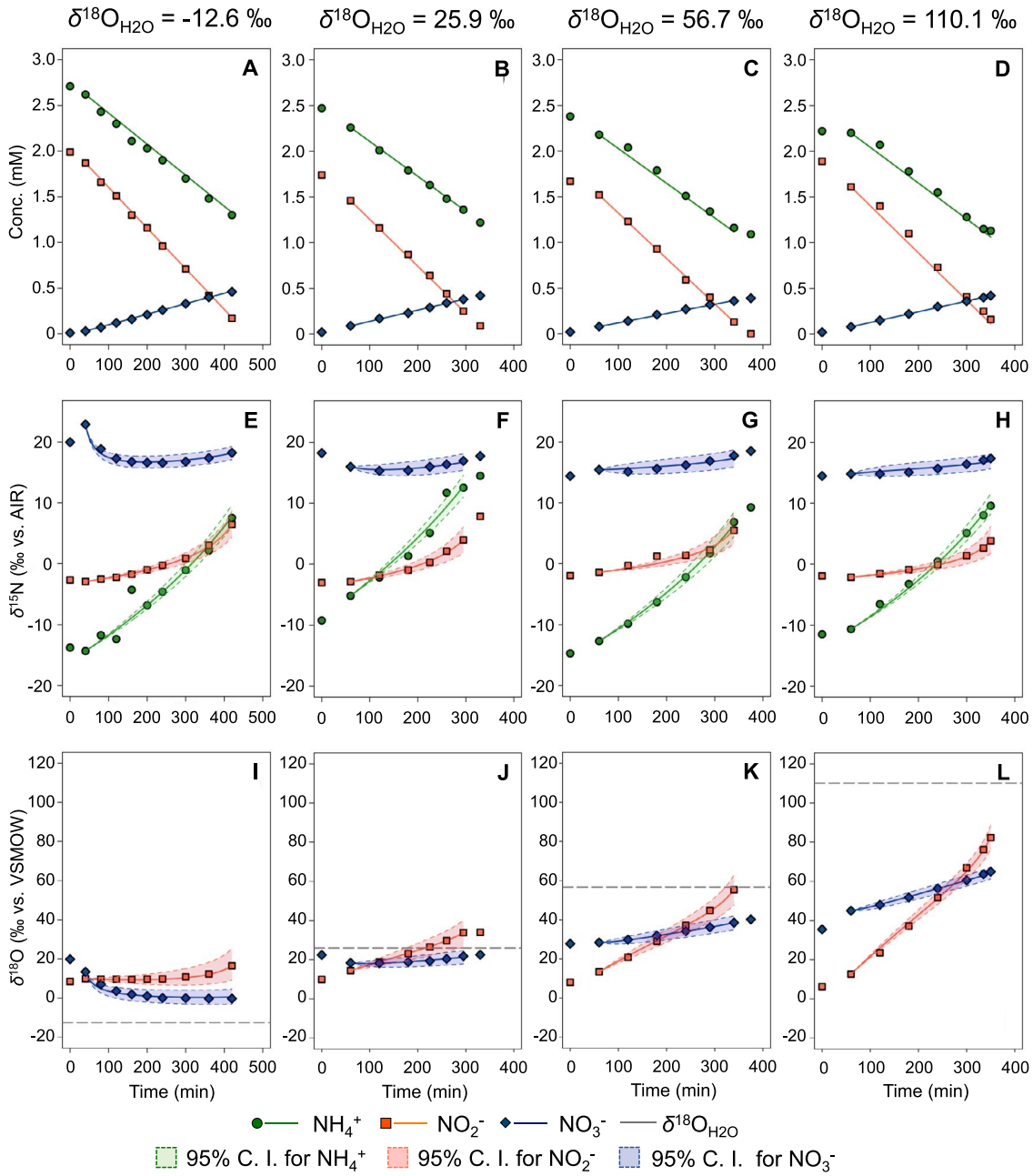

Figure 2. Changes in concentrations and nitrogen and oxygen isotope ratios of nitrogen compounds over time during anammox by "*Ca*. Scalindua sp." in typical batch culture experiments with different $\delta^{18}O_{H2O}$ of growth media. We adjusted the $\delta^{18}O_{H_2O}$ in the medium to four different values; −12.6‰ (A, E, I), 25.9‰ (B, F, J), 56.7‰ (C, G, K), and 110.1‰ (D, H, L), respectively. Concentrations (A - D), $\delta^{15}N$ (E - H), and $\delta^{18}O$ (I - L) of nitrogen compounds during the incubations. Symbols and lines represent experimental data and their model fitting by MCMC, respectively. 95% C.I. indicates 95% credible interval for estimated $\delta^{15}N$ of NH_4^+, NO_2^- and NO_3^- (E - H) and $\delta^{18}O$ of NO_2^- and NO_3^- (I - L). We performed all batch experiments in triplicate and presented only the results of the replication experiment 1. This is due to variations in sampling intervals, which depended on the activity of anammox biomass, making it difficult to merge the three-replicate data into a single figure using mean ± standard deviation. For other experimental results, please refer to the supplementary materials (Fig. S1-S4).

Nitrite was completely consumed within 295–450 min, whereas NH_4^+ remained in substantial amounts across all batch cultures (Fig. 2 A - D). Similar results were observed in three independent batch cultures (Figs. S1-S4 A - C), demonstrating the reproducibility of this study.

$\delta^{15}N$ dynamics of nitrogen compounds

$\delta^{15}N_{NH4+}$ steadily increased during the anammox reaction, indicating preferential consumption of the ^{14}N isotope of NH_4^+ i.e. normal kinetic isotope effect (Fig. 2 E-H and Figs. S1-S4 D - F). $\delta^{15}N_{NO2-}$ increased exponentially at the end of experiments, whereas $\delta^{15}N_{NO3-}$ decreased slightly at the beginning and increased to larger values at the end of all experiments. $\delta^{15}N_{NO2-}$ was affected by both NO_2^- reduction to N_2 and NO_2^- oxidation to NO_3^- (Fig. 1). The $\delta^{15}N$ of the newly produced NO_3^- was much higher than $\delta^{15}N_{NO2-}$ in all experiments, indicating that the ^{15}N isotope of NO_2^- was preferentially incorporated into NO_3^-, i.e. the inverse isotope effect [25].

Anammox bacteria oxidize NO_2^- to NO_3^- and also can reverse this enzymatic reaction [55, 56]. A previous study

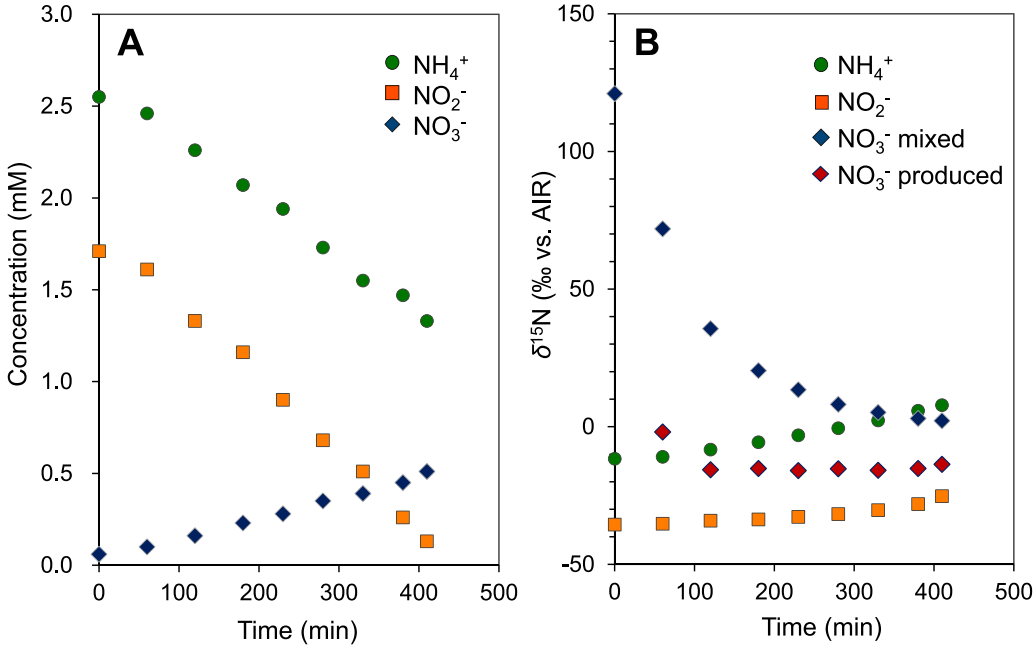

Figure 3. Changes in concentrations (A) and $\delta^{15}N$ values of nitrogen compounds (B) over time during anammox batch culture experiments with ^{15}N-poor nitrite (ACROS; $\delta^{15}N_{NO2-} = -35.5‰$) and ^{15}N-rich nitrate (USGS32; $\delta^{15}N_{NO3-} = 180‰$). In panel B, the $\delta^{15}N_{NO3-\ mixed}$ represents the measured $\delta^{15}N$ value of mixed NO_3^- (USGS32 and newly produced NO_3^-), and the $\delta^{15}N_{NO3-\ produced}$ represents the calculated $\delta^{15}N$ value of newly produced NO_3^- using a following equation: $\delta^{15}N_{NO3-\ produced} = (C_{t=t} \times \delta^{15}N_{NO3-\ t=t} - C_{t=0} \times \delta^{15}N_{NO3-\ t=0}) / (C_{t=t} - C_{t=0})$. According to this equation, the $\delta^{15}N_{NO3-\ produced}$ at t = 0 cannot be plotted because it is calculated from the difference from the initial value.

demonstrated that N isotope exchange between NO_2^- and NO_3^- ($^{15}\varepsilon_{NO2-\leftrightarrow\square NO3-} = -60.5‰$) occurred rapidly during the early growth phase [23]; however, this phenomenon was not consistently observed in their study or in our previous study [24]. To investigate N isotope exchange between NO_2^- and NO_3^-, we conducted a batch culture experiment using ^{15}N-poor NO_2^- (ACROS; $\delta^{15}N_{NO2-} = -35.5‰$) and ^{15}N-rich NO_3^- (USGS32; $\delta^{15}N_{NO3-} = 180‰$), along with unlabeled water ($\delta^{18}O_{H2O} = -12.6‰$). Given the large initial $\delta^{15}N$ difference between NO_2^- and NO_3^- (−215.5‰), any occurrence of N isotope exchange would be expected to induce an abrupt change in $\delta^{15}N_{NO2-}$ and $\delta^{15}N_{NO3-}$ during the anammox reaction.

The simultaneous consumption of NH_4^+ and NO_2^-, along with the formation of NO_3^-, was observed, aligning with the previously reported anammox stoichiometry (Fig. 3A). Approximately 0.45 mM of NO_3^- was newly produced from ^{15}N-poor NO_2^-. At t = 0, $\delta^{15}N_{NO3-}$ was lower than the original N isotopic ratio of USGS32 (180‰) and subsequently decreased asymptotically over time as NO_3^- was generated from^{15}N-poor NO_2^- (Fig. 3B). No abrupt changes in $\delta^{15}N_{NO2-}$ or $\delta^{15}N_{NO3-}$ were observed throughout the anammox reaction. The N isotope ratio of the newly produced NO_3^- ($\delta^{15}N_{NO3-\ produced}$) was calculated using the following equation.

$$\delta^{15}N_{NO3-\ produced} = (C_{t=t} \times \delta^{15}N_{NO3-\ t=t} - C_{t=0} \times \delta^{15}N_{NO3-\ t=0}) / (C_{t=t} - C_{t=0}).$$

The background NO_3^- concentration and $\delta^{15}N_{NO3-}$ in the artificial seawater were 0.02 mM and 20‰, respectively. After mixing 800 ml of artificial seawater with 8 ml of USGS32 (5 mM NO_3^-, $\delta^{15}N = 180‰$), the NO_3^- concentration and $\delta^{15}N$ of mixed NO_3^- at t = 0 were measured as 0.06 mM and 126‰, respectively. These values were in close agreement with the calculated estimates. Thus, the initial decrease in $\delta^{15}N_{NO3-\ produced}$ is likely due to dilution by NO_3^- present in the artificial seawater (Fig. 3B). In addition, NO_3^- production is minimal at the early stage of batch culture, making $\delta^{15}N_{NO3-\ produced}$ highly susceptible to errors in concentration and N isotope measurements.

Nitrogen isotope exchange between NO_2^- and NO_3^- was observed only during the initial, low-activity growth phase but was negligible in the later phase when anammox activity was fully established [23]. In all batch experiments conducted in this study, active and stoichiometrically balanced anammox reactions were initiated without distinct lag phases. Consequently, no significant N isotope exchange between NO_2^- and NO_3^- was observed, and it was therefore excluded from the subsequent numerical model simulation used to estimate nitrogen and oxygen isotope effects.

Nitrogen isotope effects ($^{15}\varepsilon$)

The kinetic nitrogen isotope effects ($^{15}\varepsilon$) for each reaction pathway were estimated using a numerical model based on Bayesian estimation, implemented with a MCMC algorithm (Fig. 1, Table 1A, Table S1A). The model simulations achieved highly successful curve-fitting across all experiments (Fig. 2 E - H and Figs. S1-S4 D - F). The mean value of $^{15}\varepsilon_{NH4+\rightarrow N2}$ was 30.9 ± 3.3‰ (mean ± SD), in good agreement with the values obtained from continuous culture experiments of "*Ca.* Scalindua sp." ($^{15}\varepsilon_{NH4+\rightarrow N2} = 32.7 \pm 0.7‰$) [24] and the value from batch culture experiments of "*Ca.* Kuenenia stuttgartiensis" ($^{15}\varepsilon_{\ NH4+\rightarrow N2} = 23.5 \sim 29.1‰$) [23]. The mean values of $^{15}\varepsilon_{NO2-\rightarrow N2}$ and $^{15}\varepsilon_{NO2-\rightarrow NO3^-}$ were 9.7 ± 1.7‰ and −17.3 ± 1.2‰, respectively. These values are smaller than the reported values of "*Ca.* Scalindua sp." ($^{15}\varepsilon_{NO2-\rightarrow N2} = 19.9 \pm 1.7‰$ and $^{15}\varepsilon_{NO2-\rightarrow NO3-} = -30.1 \pm 3.0‰$) [24]. This difference may have resulted from differences in growth conditions (water used for the culture medium, the concentrations of NH_4^+ and NO_2^-, and anammox activity) and cultivation methods (batch culture vs. continuous culture).

To assess the validity of the model simulation results, we also determined the kinetic nitrogen isotope effects of

Table 1. Summary of nitrogen (**A**) and oxygen isotope effects and a reaction rate constant ($k_{eq,\ AMX}$) for anammox-mediated oxygen isotope exchange between NO_2^- and H_2O (**B**) during anammox metabolism determined from batch culture experiments with different $\delta^{18}O_{H2O}$ media using a newly developed numerical model implemented with a MCMC algorithm.

A

$\delta^{18}O_{H2O}$ of medium (‰)	n $^{15}\varepsilon_{NH4+\rightarrow N2}$ (‰)	$^{15}\varepsilon_{AMO}$ $^{15}\varepsilon_{NO2-\rightarrow N2}$ (‰)	$^{15}\varepsilon_{NIR}$ $^{15}\varepsilon_{NO2-\rightarrow NO3-}$ (‰)	$^{15}\varepsilon_{NXR}$
−12.6	3	30.2 ± 3.1	11.7 ± 0.6	−16.9 ± 1.0
25.9	3	33.7 ± 3.0	10.2 ± 1.1	−17.0 ± 1.0
56.7	3	28.9 ± 1.8	8.4 ± 1.3	−17.6 ± 1.4
110.1	3	30.9 ± 3.0	8.5 ± 0.7	−17.9 ± 1.0
Average	12	30.9 ± 3.3	9.7 ± 1.7	−17.3 ± 1.2

B

$\delta^{18}O_{H2O}$ of medium (‰)	n	$^{18}\varepsilon_{NIR}$ $^{18}\varepsilon_{NO2-\rightarrow N2}$ ‰	$^{18}\varepsilon_{NXR}$ $^{18}\varepsilon_{NO2-\rightarrow NO3-}$ (‰)	$^{18}\varepsilon_{H2O}$ (‰)	$k_{eq,\ AMX}$ ($\times 10^{-2}$ h^{-1})
−12.6	3	10.6 ± 2.5	−2.9 ± 1.9	19.2 ± 3.8	13.56 ± 5.38
25.9	3	12.1 ± 2.5	−6.3 ± 2.5	17.7 ± 4.3	8.44 ± 4.63
56.7	3	13.8 ± 2.6	−9.8 ± 2.5	17.3 ± 4.2	11.28 ± 2.54
110.1	3	16.1 ± 3.2	−11.0 ± 2.1	16.4 ± 4.0	12.44 ± 3.13

The values are the overall mean and SD of the three posteriors obtained by each batch experiment replicate.

NH_4^+ oxidation, NO_2^- reduction, and NO_2^- oxidation using a closed-system Rayleigh model, as previously described [23] (Table S2, Figs. S5-S7). The calculated $^{15}\varepsilon$ values for NH_4^+ oxidation and NO_2^- oxidation ($^{15}\varepsilon_{NH4+\rightarrow N2} = 27.5‰ \sim 33.3‰$ and $^{15}\varepsilon_{NO2-\rightarrow NO3-} = -17.7‰ \sim -19.0‰$) (Table S2) closely matched those obtained from our model fitting (Table 1A), whereas $^{15}\varepsilon_{NO2-\rightarrow N2}$ ranged from 0.5‰ to 2.4‰ ($\delta^{15}N_{NO2-}$ based) and from 1.5‰ to 8.6‰ ($\delta^{15}N_{NO3-}$ based) (Table S2), which were slightly lower than the values obtained from the model fitting (8.4‰ ∼ 11.7‰; Table 1A). A similar discrepancy in $^{15}\varepsilon$ estimations has been reported previously [23], however, the exact reason is currently unknown.

$\delta^{18}O$ dynamics of nitrogen compounds

During the anammox reaction, $\delta^{18}O_{NO2-}$ values rapidly approached equilibrium between NO_2^- and H_2O within 6–7 hours of incubation in high $\delta^{18}O_{H2O}$ media (Fig. 4A and Fig. S8). In contrast, in abiotic conditions, the equilibrium was achieved within ca. 650 h (Fig. S8) [45]. This indicates that "*Ca.* Scalindua sp." significantly promoted O isotope exchange between NO_2^- and H_2O. This is probably due to three reasons: (i) the lower pH in anammoxosome, (ii) the reversibility of NO_2^- oxidation reaction, and (iii) the reversibility of NO_2^- reduction reaction, as explained in detail below. First, an anammox reaction occurs within anammoxosome, the pH of which is known to be around 6 [57], more than one unit lower than the culture medium (pH ≈ 7.5). The oxygen exchange rate has been reported to increase as the pH decreases [22]. At 30°C, the rate of abiotic oxygen exchange k_{eq} was estimated to be 4.39×10^{-2} h^{-1} at pH 6 and 1.13×10^{-2} h^{-1} at pH 7.5 [22]. These values indicate considerable differences in the O isotope exchange between NO_2^- and H_2O within the anammoxosome. Second, when NO_2^- is oxidized to NO_3^-, first a complex of the enzyme nitrite oxidoreductase and O atom derived from H_2O is formed, then this enzyme-oxygen complex combines with NO_2^- to form a transition state [28, 58]. This transition state (temporarily containing three O atoms) can either cleave the enzyme to form NO_3^- or lose one of the three O atoms and decompose back to NO_2 [28, 58]. If the original O atom of NO_2^- is lost during the reverse reaction, it is replaced by an O atom of H_2O. Third, in the NO_2^- reduction reaction by "*Ca.* Scalindua sp.", NO_2^- is first reduced to nitric oxide (NO), which is then combined with NH_4^+ and converted to hydrazine (N_2H_4) [59]. Because the latter hydrazine synthesis is the rate-limiting step [1], NO may accumulate slightly in the anammoxozome [60] and some of which may acquire O atoms from H_2O and be re-oxidized back to NO_2^-. This reverse reaction would further promote O isotope exchange between NO_2^- and H_2O. Similar microbially facilitated O isotope exchange between NO_2^- and H_2O has also been reported in aerobic AOB [27] and archaea (AOA) [29], as well as nitrite-oxidizing bacteria (NOB) [28, 30, 31].

The $\delta^{18}O_{NO3-}$ values appeared to depend on the $\delta^{18}O_{H2O}$ media (Fig. 4B). When the $\delta^{18}O_{H2O}$ media value was −12.6‰, the $\delta^{18}O_{NO3-}$ decreased from 15‰ to −0.3‰. Similarly, at $\delta^{18}O_{H2O}$ values of 25.9‰, 56.7‰, and 110.1‰, the final $\delta^{18}O_{NO3-}$ values were approximately 22‰, 42‰, and 64‰, respectively. These results indicate that the $\delta^{18}O_{NO3-,\ produced}$ are gradually approaches equilibrium with the $\delta^{18}O_{H2O}$ medium by incorporating O atoms from water, although full equilibrium has not yet been reached. The change in $\delta^{18}O_{NO2-}$ occurred more rapid than that in $\delta^{18}O_{NO3-,\ produced}$ (Fig. S9), suggesting that O isotope exchange between NO_2^- and H_2O played a significant role.

Dependence of $\delta^{18}O_{NO2-}$ and $\delta^{18}O_{NO3-}$ on $\delta^{18}O_{H2O}$

The values of $\delta^{18}O_{NO2-,\ final}$ and $\delta^{18}O_{NO3-,\ final}$ at the end of incubation (when NO_2^- was almost consumed) were plotted against $\delta^{18}O_{H2O}$, and both showed the same linear relationship with the same slope of 0.56 (Fig. 5). According to the definition of $\delta^{18}O_{NO3-,\ final}$ [22, 27], this indicates that 34% of O atoms in NO_2^- were exchanged with H_2O before oxidation to NO_3^- (see Supplementary materials for details of this calculation). Additionally, one O atom was incorporated from H_2O into NO_2^- during its oxidation to NO_3^- [27, 61]. These findings suggest that, depending on the extent of equilibration, all three O atoms in the resulting NO_3^- may carry the isotopic signature of water. As

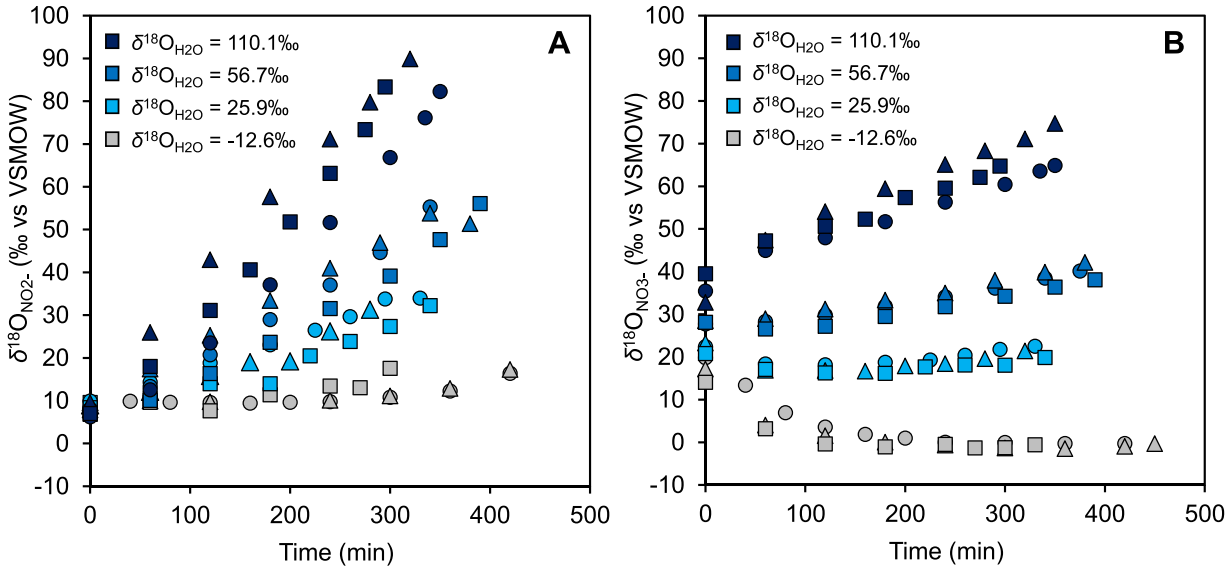

Figure 4. Summary of changes in $\delta^{18}O$ values of NO_2^- (A) and NO_3^- (B) over time during anammox batch culture experiments with different $\delta^{18}O_{H2O}$ of growth media (−12.6‰, 25.9‰, 56.7‰, and 110.1‰). We conducted the batch culture experiments in triplicates for each $\delta^{18}O_{H2O}$ media (1st: Circle, 2nd: Triangle, 3rd: Square).

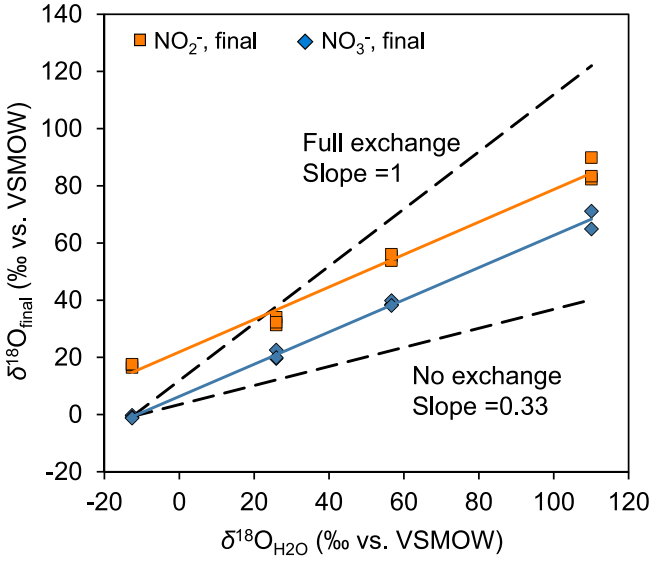

Figure 5. Relationship between final values of $\delta^{18}O_{NO2-}$ and $\delta^{18}O_{NO3-}$ and $\delta^{18}O_{H2O}$ media. The final values of $\delta^{18}O_{NO2-, final}$ and $\delta^{18}O_{NO3-, final}$ at the end of incubation (when NO_2^- was almost consumed) were plotted against $\delta^{18}O_{H2O}$. All triplicate data were plotted in this figure. The dashed black lines indicate estimated full exchange (slope = 1, 100% incorporation) and no exchange (33% incorporation) for NO_3^-. The slopes of the regression lines of $\delta^{18}O_{NO2-, final}$ and $\delta^{18}O_{NO3-, final}$ were 0.568 and 0.563, respectively, indicating that 34% of O atoms in NO_2^- were exchanged with H_2O before oxidation to NO_3^- (see supplementary materials for details of this calculation).

a result, both $\delta^{18}O_{NO2-}$ and $\delta^{18}O_{NO3-}$ in the anammox reaction were strongly dependent on $\delta^{18}O_{H2O}$, even though their oxygen isotopic systematics are different: $\delta^{18}O_{NO3-}$ is influenced by isotopic fractionation of NO_2^- oxidation and O uptake from H_2O during NO_2^- oxidation, whereas $\delta^{18}O_{NO2-}$ is influenced by isotopic fractionations of NO_2^- oxidation, NO_2^- reduction, and O isotope exchange between NO_2^- and H_2O (Fig. 1). The specific mechanism underlying why $\delta^{18}O_{NO2-, final}$ and $\delta^{18}O_{NO3-, final}$ exhibit the same correlation (slope) with $\delta^{18}O_{H2O}$ remains unknown at this time.

Based on these observations, we incorporated the reaction rate constants ($k_{eq, abio}$ and $k_{eq, AMX}$) and equilibrium isotope effects ($^{18}\varepsilon_{eq, abio}$ and $^{18}\varepsilon_{eq, AMX}$) of both abiotic and anammox-mediated O isotope exchange processes into the numerical model to simulate O isotope exchange between NO_2^- and H_2O via anammox (Fig. 1). To determine $k_{eq, AMX}$ and $^{18}\varepsilon_{eq, AMX}$ using the numerical model, we assumed that $^{18}\varepsilon_{eq, AMX}$ was identical to the abiotic equilibrium isotope effect ($^{18}\varepsilon_{eq, abio}$ = 11.9‰) [45]. This assumption is based on the principle that an enzyme does not alter the equilibrium point but can accelerate the rate at which equilibrium is reached [28].

Numerical model simulation

A closed-system Rayleigh model is not applicable to the oxygen isotope systematics of anammox, as multiple reactions including O isotope exchange between NO_2^- and H_2O influence the oxygen isotopic composition of NO_2^- and NO_3^- (Fig. 1). The Rayleigh model is designed for unidirectional reactions with a single product and relies on certain approximations to maintain linearity. Therefore, the oxygen isotope effects ($^{18}\varepsilon$) during anammox were directly estimated using a Bayesian approach in a numerical model implemented with a MCMC algorithm. The MCMC algorithm is a powerful tool capable of estimating multiple parameters and their uncertainties through iterative random sampling. This method does not require any approximations and enables the validation of various types of models. The formulation of the nitrogen and oxygen isotopic model of the anammox reaction is described in the Supplementary Materials.

We estimated three kinetic O isotope effects ($^{18}\varepsilon_{NO2- \rightarrow N2}$, $^{18}\varepsilon_{NO2- \rightarrow NO3-}$ and $^{18}\varepsilon_{H2O}$) as well as the rate constant for O isotope exchange between NO_2^- and H_2O ($k_{eq, AMX}$) associated with anammox reaction using the numerical model with default parameter settings (Table S4). The curve-fitting results, along with 95% confidence intervals for temporal changes in concentrations and oxygen isotopic ratios of nitrogen compounds in each batch experiment, are presented in Figs. 2 I - L and Figs. S1-S4 G - I.

Oxygen isotope effects ($^{18}\varepsilon$)

The estimated oxygen isotope effects ($^{18}\varepsilon$) and reaction rate constants for anammox-mediated O isotope exchange between NO_2^- and H_2O ($k_{eq, AMX}$) are summarized in Fig. 6, Table 1B and Table S1B. The overall posterior means ± SD of $k_{eq, AMX}$

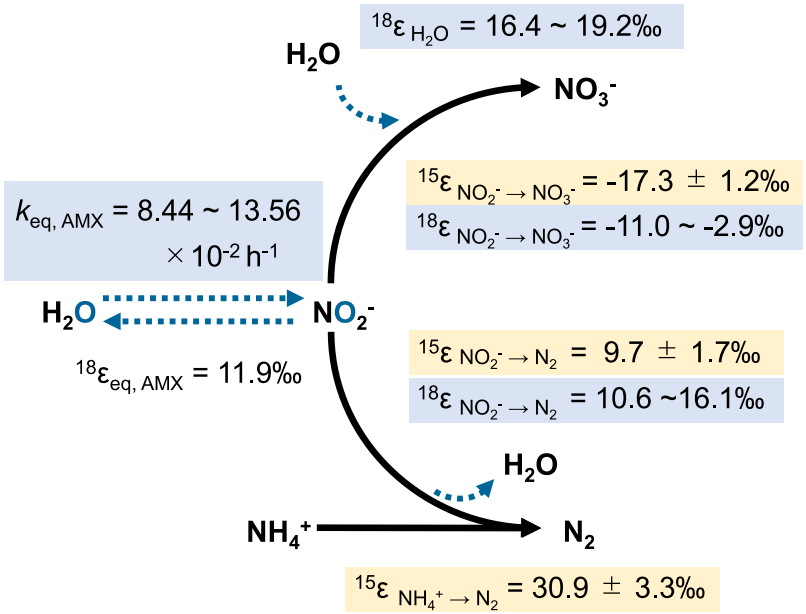

Figure 6. Summary of N and O isotope effects associated with anammox. These N and O isotope effects were determined at different $\delta^{18}O_{H2O}$ of growth media (−12.6‰, 25.9‰, 56.7‰, and 110.1‰) in this study. The values of nitrogen isotope effects are overall mean and SD of twelve posteriors (including different $\delta^{18}O_{H2O}$ of growth media) obtained from a numerical model implemented with a MCMC algorithm. The values of oxygen isotope effects are the ranges of overall means of three posteriors based on different $\delta^{18}O_{H2O}$ of growth media. The equilibrium isotope effect ($^{18}\varepsilon_{eq, AMX}$) for anammox-mediated oxygen isotope exchange between NO_2^- and H_2O was assumed to be identical to $^{18}\varepsilon_{eq, abio}$ (11.9‰), as previously determined [45].

determined by 100 000 iterations with the MCMC algorithm were 13.56 ± 5.38, 8.44 ± 4.63, 11.28 ± 2.54 and 12.44 ± 3.13 (× 10^{-2} h^{-1}) at $\delta^{18}O_{H2O}$ of −12.6‰, 25.9‰, 56.7‰ and 110.1‰, respectively (Table 1B). These $k_{eq, AMX}$ values were 7.5 to 12 times higher than the reaction rate constant of abiotic O isotope exchange ($k_{eq, abio} = 1.13 \times 10^{-2}$ h^{-1}) [45]. The kinetic O isotope effects during NO_2^- reduction to N_2, $^{18}\varepsilon_{NO2- \rightarrow N2}$, were 10.6 ± 2.5‰, 12.1 ± 2.5‰, 13.8 ± 2.6‰ and 16.1 ± 3.2‰ at $\delta^{18}O_{H2O}$ of −12.6‰, 25.9‰, 56.7‰ and 110.1‰, respectively (Table 1B). The O isotope effects of NO_2^- reduction catalyzed by copper-containing nitrite reductase (Cu-NIR) and cytochrome cd_1-containing nitrite reductase (Fe-NIR) (both catalyse the reduction of NO_2^- to NO) were determined for several denitrifying bacterial strains [52]. Denitrifier strains with Fe-NIR exhibited a slightly larger O isotope effect ($^{18}\varepsilon_{NO2- \rightarrow N2} = 6 \pm 2$‰) than denitrifier strains with Cu-NIR ($^{18}\varepsilon_{NO2- \rightarrow N2} = 2 \pm 2$‰) [52]. "*Ca.* Scalindua sp." showed larger O isotope effects ($^{18}\varepsilon_{NO2- \rightarrow N2}$ = 10.6 to 16.1‰) than denitrifier strains with Fe-NIR [52]. The identity and function of nitrite reductase in "*Ca.* Scalindua sp." remain under debate [62], and further research is needed to elucidate its details.

For NO_2^- oxidation to NO_3^-, the inverse isotope effect ($^{18}\varepsilon_{NO2- \rightarrow NO3-}$) was determined as −2.9 ± 1.9‰, −6.3 ± 2.5‰, −9.8 ± 2.5‰ and − 11.0 ± 2.1‰ at $\delta^{18}O_{H2O}$ values of −12.6‰, 25.9‰, 56.7‰, and 110.1‰, respectively (Table 1B). Nitrite-oxidizing bacteria (NOB) also exhibited inverse kinetic O isotope effects ($^{18}\varepsilon_{NO2- \rightarrow NO3-}$ = −1.3 ± 0.4‰ to −8.2 ± 2.6‰) [28]. The kinetic O isotope effect associated with the incorporation of O atom from H_2O during NO_2^- oxidation to NO_3^-, $^{18}\varepsilon_{H2O}$, was 19.2 ± 3.8‰, 17.7 ± 4.3‰, 17.3 ± 4.2‰, and 16.4 ± 4.0‰ when $\delta^{18}O_{H2O}$ was 12.6‰, 25.9‰, 56.7‰, and 110.1‰, respectively (Table 1B). The $^{18}\varepsilon_{H2O}$ values were positive, indicating a normal kinetic O isotope effect, similar to those observed in NOB [28]. $H_2{}^{16}O$ were preferentially incorporated into NO_3^-, resulting in the $\delta^{18}O_{NO3-}$ values lower than the $\delta^{18}O_{NO2-}$ values at the end of all anammox batch experiments (Figs. 2 I - L and Figs. S1-S4 G - I).

Evaluation of estimated parameters

The estimated parameters and their 95% confidence interval are summarized in Fig. S10. The variability in the estimated O isotope effects may be attributed to the fact that $\delta^{18}O_{NO2-}$ and $\delta^{18}O_{NO3-}$ converged with the $\delta^{18}O_{H2O}$ at rates significantly faster than currently expected (Fig. 4 and Fig. S8). This finding suggests the presence of unknown pathways or processes facilitating O atom exchange between H_2O and NO_2^-. To characterize the unexpectedly rapid anammox-mediated O isotope exchange between NO_2^- and H_2O, we introduced a reaction rate constant ($k_{eq, AMX}$). Pairs plot analyses revealed a linear correlation between $k_{eq, AMX}$ and $^{18}\varepsilon_{NO2- \rightarrow N2}$ (Fig. S11). To assess the influence of $k_{eq, AMX}$ on the estimation of other parameters ($^{18}\varepsilon_{NO2- \rightarrow N2}$, $^{18}\varepsilon_{NO2- \rightarrow NO3-}$, and $^{18}\varepsilon_{H2O}$), model simulations were performed with $k_{eq, AMX}$ values fixed at 10.8, 12.0, 13.2, 15.0, or 18.0 (×10^{-2} h^{-1}) (Fig. S12). When $k_{eq, AMX}$ was fixed at 15.0 × 10^{-2} h^{-1}, the narrowest ranges, showing minimal dependence on $\delta^{18}O_{H2O}$, were obtained for $^{18}\varepsilon_{NO2- \rightarrow N2}$ (11.2 ± 1.2‰, 7.8 ± 1.6‰, 9.3 ± 1.7‰ and 11.2 ± 3.5‰) and $^{18}\varepsilon_{H2O}$ (19.0 ± 3.9‰, 18.0 ± 4.3‰, 17.1 ± 4.3‰ and 17.5 ± 4.3‰) at $\delta^{18}O_{H2O}$ values of −12.6‰, 25.9‰, 56.7‰, and 110.1‰, respectively (Fig. S12 A and C), whereas the variations in $k_{eq, AMX}$ did not affect $^{18}\varepsilon_{NO2- \rightarrow NO3-}$ (Fig. S12B). To evaluate the impact of $^{18}\varepsilon_{NO2- \rightarrow NO3-}$ on the curve-fitting results for $\delta^{18}O_{NO2-}$ and $\delta^{18}O_{NO3-}$, model simulations were conducted with $^{18}\varepsilon_{NO2- \rightarrow NO3-}$ values fixed at 0‰, −5.0‰ and − 9.7‰ (Fig. S13). As $^{18}\varepsilon_{NO2- \rightarrow NO3-}$ became more negative, $\delta^{18}O_{NO3-}$ increased progressively, achieving optimal curve-fitting at $^{18}\varepsilon_{NO2- \rightarrow NO3-}$ value of −9.7‰. In batch experiments with higher $\delta^{18}O_{H2O}$ values, the stronger negative $^{18}\varepsilon_{NO2- \rightarrow NO3-}$ values may serve to compensate for the observed increase in $\delta^{18}O_{NO3-}$.

Another possible explanation for the convergence of $\delta^{18}O_{NO2-}$ and $\delta^{18}O_{NO3-}$ values toward $\delta^{18}O_{H2O}$ is the reverse reaction of NO_2^- oxidation (i.e. NO_3^- reduction or a NO_2^- transition state decomposes back to NO_2^-) facilitated by the enzyme nitrite oxidoreductase (NXR). To assess the effect of NO_2^- oxidation reversibility on

curve-fitting, we incorporated the backward flux of NO_2^- oxidation (i.e. NO_3^- reduction) into the model simulation. Model simulations were conducted using the ratio of NO_3^- reduction rate (backward flux) to NO_2^- oxidation rate (forward flux) (Fig. S14). Even under conditions assuming large backward fluxes (up to 75%), the rapid increases in $\delta^{18}O_{NO3\text{-}}$ and $\delta^{18}O_{NO2\text{-}}$ over time, particularly the convergence of $\delta^{18}O_{NO2\text{-}}$ with $\delta^{18}O_{NO2\text{-},eq}$, could not be reproduced. The simulated reversibility (up to 75%) was significantly greater than previously observed reverse reactions mediated by NXR in anammox bacteria [63]. This discrepancy is likely due to the relatively smaller reaction pool of NO_2^- oxidation to NO_3^- compared to NO_2^- reduction to N_2 in the anammox metabolism. Because the reversibility of NO_2^- oxidation has a limited effect on $\delta^{18}O_{NO_2^-}$, excluding the backward flux of NO_2^- oxidation from parameter estimation in the model simulations is a reasonable approach.

Oxygen isotope exchange between NO_2^- and H_2O associated with anammox can diminish or overwrite the isotope signals of NO_2^- reduction and oxidation, yielding NO_3^- with $\delta^{18}O$ values closely aligned with those of ambient water. A similar influence of $\delta^{18}O_{H2O}$ on $\delta^{18}O_{NO3\text{-}}$ was observed in nitrification [31]. The $\delta^{18}O$ values of NO_3^- produced via NO_2^- oxidation could not be explained solely by a 2: 1 incorporation ratio of water and molecular O atoms [31]. Instead, these values were largely modulated by O exchange between H_2O and NO_2^-, as well as kinetic and equilibrium isotope effects influencing O atom incorporation from both sources [31]. Consequently, $\delta^{18}O_{NO3\text{-}}$ generally converges with $\delta^{18}O_{H2O}$, and the reported $\delta^{18}O_{NO3\text{-}}$ values may not necessarily reflect the isotope signature of nitrification [31]. Anoxic incubation experiments using natural sediments containing both NO_2^-—oxidizing and denitrifying microorganisms revealed that $\delta^{18}O_{NO3\text{-}}$ was significantly affected by the extent of O atom incorporation from ambient H_2O [64]. This suggests that O atom incorporation into NO_3^- by NO_2^-—oxidizing microorganism can override the original O isotope signature of denitrification [64].

Influence of $\delta^{18}O_{H2O}$ on NO_3^- $\Delta\delta^{18}O$: $\Delta\delta^{15}N$ trajectory during anammox reaction (model simulation excises)

NO_3^- is the primary bioavailable form of nitrogen in the ocean, and its natural abundance and stable isotope ratios of N and O ($\delta^{15}N_{NO3\text{-}}$ and $\delta^{18}O_{NO3\text{-}}$) serve as valuable markers for tracking the biogeochemical conversion processes of NO_3^- in the natural environment. Early studies suggested that the heavy O and N isotopes in NO_3^- are proportionally enriched during denitrification and that the N and O isotopic effects of NO_3^- are nearly identical (i.e. $^{18}\varepsilon$: $^{15}\varepsilon = 1$) [65–67]. Deviations from the expected trajectory of NO_3^- $\Delta\delta^{18}O$: $\Delta\delta^{15}N = 1$ have been attributed to the inverse kinetic isotope effect associated with canonical nitrite oxidation [14, 50, 67].

To evaluate the impact of $\delta^{18}O_{H2O}$ on the trajectories of $\Delta\delta^{18}O_{NO3\text{-}}$: $\Delta\delta^{15}N_{NO3\text{-}}$ for anammox, model simulations were performed using the N and O isotope effects determined in this study, with $\delta^{18}O_{H2O}$ values ranging from −7.7‰ to 1.8‰ (refer to Supplementary Materials text for details on the parameter setting). It was assumed that complete isotopic equilibrium had been established between NO_2^- and H_2O. All the parameters used in the model simulation exercises are provided in Table S5.

Model simulation revealed that $\delta^{18}O_{H2O}$ significantly influences the trajectories of $\Delta\delta^{18}O_{NO3\text{-}}$: $\Delta\delta^{15}N_{NO3\text{-}}$ even within a relatively small range of $\delta^{18}O_{H2O}$ values ($\delta^{18}O_{H2O}$ = −7.7‰ to 1.8‰) (Fig. 7). Under these simulation settings (Table S5), the $\delta^{18}O$ value of NO_3^- produced from NO_2^- oxidation via anammox is directly

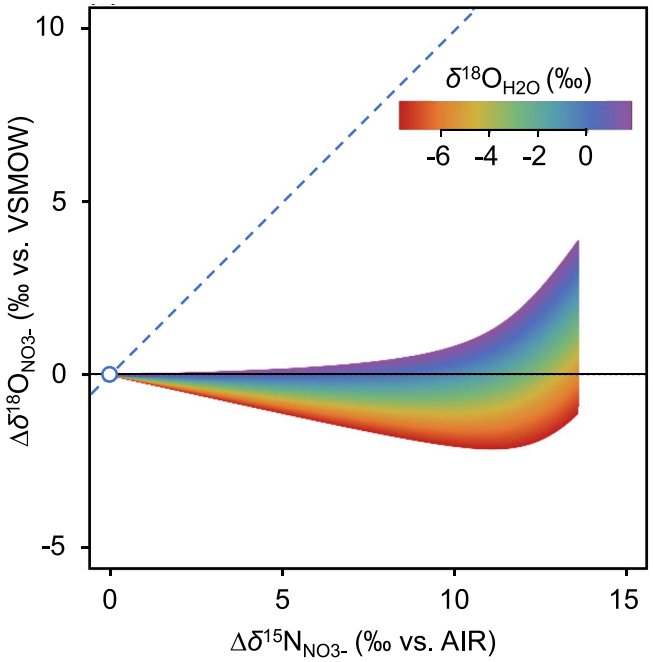

Figure 7. Influence of $\delta^{18}O_{H2O}$ on $\Delta\delta^{18}O_{NO3\text{-}}$: $\Delta\delta^{15}N_{NO3\text{-}}$ as predicted by model simulation. Model simulations were performed using $\delta^{18}O_{H_2O}$ values ranging from −7.7‰ to 1.8‰, with parameters provided in Table S5. Complete isotopic equilibrium between NO_2^- and H_2O was assumed. $\Delta\delta^{18}O_{NO3\text{-}}$ ($\delta^{18}O_{NO3\text{-}}$ - $\delta^{18}O_{NO3\text{-,initial}}$) was plotted against the corresponding $\Delta\delta^{15}N_{NO3\text{-}}$ ($\delta^{15}N_{NO3\text{-}}$ - $\delta^{15}N_{NO3\text{-,initial}}$) for varying $\delta^{18}O_{H2O}$ values. The dotted line represents the trajectory of $\Delta\delta^{18}O_{NO3\text{-}}$: $\Delta\delta^{15}N_{NO3\text{-}} = 1$.

linked to $\delta^{18}O_{H2O}$ (Fig. 3 and Fig. S9). Consequently, the trajectory of NO_3^- $\Delta\delta^{18}O$: $\Delta\delta^{15}N$ remained below 0.3, regardless of $\delta^{18}O_{H2O}$, due to lower $\delta^{18}O_{NO3\text{-}}$ values (Fig. 7). This suggests that the inverse kinetic N and O isotope effects associated with anammox-driven NO_2^- oxidation, coupled with the rapid exchange of O atom between NO_2^- and H_2O, result in a deviation from the expected trajectory of NO_3^- $\Delta\delta^{18}O$: $\Delta\delta^{15}N = 1$, similar to that observed in canonical nitrite oxidation.

In microbial NO_3^- reduction systems, several studies have reported that NO_3^- reduction mediated by Nap (periplasmic nitrate reductase) increases the $\delta^{15}N$ of residual NO_3^- relative to $\delta^{18}O$, resulting in a trajectory of NO_3^- $\Delta\delta^{18}O$: $\Delta\delta^{15}N \approx 0.5$ [65, 67–69]. Conversely, a recent study found that the trajectory of NO_3^- $\Delta\delta^{18}O$: $\Delta\delta^{15}N$ remained stable at ~1, even in denitrifying enrichment cultures with varying levels of NapA and NarG expression [70]. These contrasting findings indicate that uncertainties remain in quantifying the contributions of NO_2^- oxidation by anammox and NO_3^- reduction by Nap based solely on the NO_3^- $\Delta\delta^{18}O$: $\Delta\delta^{15}N$, emphasizing the need for further research.

In conclusion, because "*Ca.* Scalindua sp." significantly enhanced oxygen isotope exchange between NO_2^- and H_2O, we proposed a new rate constant for anammox-mediated oxygen isotope exchange ($k_{eq,AMX} = 8.44 \sim 13.56 \times 10^{-2}$ h^{-1}), incorporated it into a newly developed numerical model, and determined the previously unexplored oxygen isotope effects ($^{18}\varepsilon$) during anammox using a highly enrichment culture of the marine representative *Ca.* Scalindua sp. Previous studies have shown that the $\delta^{18}O$ of NO_3^- (where two of the three O atoms in NO_3^- are derived from water) produced in aerobic nitrification generally converges toward the $\delta^{18}O$ of ambient water due to isotopic equilibrium between NO_2^- and H_2O and kinetic isotope effects during oxygen uptake from molecular oxygen and H_2O. The

present study further demonstrates that $\delta^{18}O_{NO3-}$ converges near the $\delta^{18}O$ of ambient water as a result of significant O isotope exchange between NO_2^- and H_2O, even during the anaerobic oxidation of NO_2^- to NO_3^- (where only one O atom is incorporated from H_2O into NO_3^-) in anammox metabolism. Therefore, caution is needed when using $\delta^{18}O_{NO3-}$ and $\delta^{18}O_{NO2-}$ as geochemical markers to evaluate their potential contribution to fixed nitrogen losses in the ocean, as the isotope signals of anammox and denitrification reactions may be altered even under anoxic conditions. Further studies are required to determine the extent to which anammox-mediated oxygen isotope exchange occurs in natural environments and its impact on $\delta^{18}O_{NO3-}$ and $\delta^{18}O_{NO2-}$.

Acknowledgements

We would like to thank S. D. Wankel and Karen L. Casciotti for the calibration of our in-house NO_2^- standards and discussion for experimental design.

Author contributions

Kanae Kobayashi (Data curation, Formal analysis, Funding acquisition, Investigation, Methodology, Software, Validation, Visualization, Writing—original, Writing—review & editing), Kazuya Nishina (Formal analysis, Investigation, Methodology, Software, Validation, Visualization), Keitaro Fukushima (Data curation, Investigation, Methodology), Yuji Onishi (Data curation, Investigation, Methodology), Akiko Makabe (Data curation, Investigation, Methodology), Mamoru Oshiki (Supervision, Writing—review & editing), Keisuke Koba (Formal analysis, Funding acquisition, Resources, Software, Supervision, Writing—review & editing), Satoshi Okabe (Conceptualization, Funding acquisition, Investigation, Resources, Supervision, Validation, Visualization, Writing—original, Writing—review & editing). These authors read and approved the final manuscript.

Supplementary material

Supplementary material is available at *The ISME Journal* online.

Conflicts of interest

None declared.

Funding

This work was financially supported by Japan Society for the Promotion of Science KAKENHI 18 J20742 (granted to KK), KAKENHI 18H04138 (KK), KAKENHI 20 K20316 (KK), KAKENHI 19H00776 (SO), KAKENHI 23H00192 (SO), and Joint Usage/Research Grant of Center for Ecological Research, Kyoto University, Grant number: 2016jurc- cer24 (KK).

Data availability

All the data underlying this manuscript are available in the main text and/or the Supplementary Materials. The R code will be available at ZENODO.

References

1. Kartal B, de Almeida NM, Maalcke WJ. *et al.* How to make a living from anaerobic ammonium oxidation. *FEMS Microbiol Rev* 2013;**37**:428–61. https://doi.org/10.1111/1574-6976.12014
2. Lotti T, Kleerebezem R, Lubello C. *et al.* Physiological and kinetic characterization of a suspended cell anammox culture. *Water Res* 2014;**60**:1–14. https://doi.org/10.1016/j.watres.2014.04.017
3. Dalsgaard T, Thamdrup B, Farías L. *et al.* Anammox and denitrification in the oxygen minimum zone of the eastern South Pacific. *Limnol Oceanogr* 2012;**57**:1331–46. https://doi.org/10.4319/lo.2012.57.5.1331
4. Kalvelage T, Jensen MM, Contreras S. *et al.* Oxygen sensitivity of anammox and coupled N-cycle processes in oxygen minimum zones. *PLoS One* 2011;**6**:e29299. https://doi.org/10.1371/journal.pone.0029299
5. Lam P, Jensen MM, Lavik G. *et al.* Linking crenarchaeal and bacterial nitrification to anammox in the Black Sea. *Proc Natl Acad Sci USA* 2007;**104**:7104–9. https://doi.org/10.1073/pnas.0611081104
6. Dalsgaard T, Canfield DE, Petersen J. *et al.* N_2 production by the anammox reaction in the anoxic water column of Golfo Dulce, Costa Rica. *Nature* 2003;**422**:606–8. https://doi.org/10.1038/nature01526
7. Thamdrup B, Dalsgaard T, Jensen MM. *et al.* Anaerobic ammonium oxidation in the oxygen-deficient waters off northern Chile. *Limnol Oceanogr* 2006;**51**:2145–56. https://doi.org/10.4319/lo.2006.51.5.2145
8. Jensen MM, Kuypers MMM, Gaute L. *et al.* Rates and regulation of anaerobic ammonium oxidation and denitrification in the Black Sea. *Limnol Oceanogr* 2008;**53**:23–36. https://doi.org/10.4319/lo.2008.53.1.0023
9. Dähnke K, Thamdrup B. Isotope fractionation and isotope decoupling during anammox and denitrification in marine sediments. *Limnol Oceanogr* 2016;**61**:610–24. https://doi.org/10.1002/lno.10237
10. Prokopenko MG, Hammond DE, Berelson WM. *et al.* Nitrogen cycling in the sediments of Santa Barbara basin and eastern subtropical North Pacific: nitrogen isotopes, diagenesis and possible chemosymbiosis between two lithotrophs (*Thioploca* and Anammox) - 'riding on a glider'. *Earth Planet Sci Lett* 2006;**242**:186–204. https://doi.org/10.1016/j.epsl.2005.11.044
11. Prokopenko MG, Hirst MB, de Brabandere L. *et al.* Nitrogen losses in anoxic marine sediments driven by *Thioploca*-anammox bacterial consortia. *Nature* 2013;**500**:194–8. https://doi.org/10.1038/nature12365
12. Babbin AR, Ward BB. Controls on nitrogen loss processes in Chesapeake Bay sediments. *Environ Sci Technol* 2013;**47**:4189–96. https://doi.org/10.1021/es304842r
13. Babbin AR, Jayakumar A, Ward BB. Organic matter loading modifies the microbial community responsible for nitrogen loss in estuarine sediments. *Microb Ecol* 2016;**71**:555–65. https://doi.org/10.1007/s00248-015-0693-5
14. Sigman DM, Granger J, DiFiore PJ. *et al.* Coupled nitrogen and oxygen isotope measurements of nitrate along the eastern North Pacific margin. *Glob Biogeochem Cycles* 2005;**19**:1–14. https://doi.org/10.1029/2005GB002458
15. Lehmann MF, Sigman DM, Berelson WM. Coupling the $^{15}N/^{14}N$ and $^{18}O/^{16}O$ of nitrate as a constraint on benthic nitrogen cycling. *Mar Chem* 2004;**88**:1–20. https://doi.org/10.1016/j.marchem.2004.02.001
16. Lehmann MF, Sigman DM, McCorkle DC. *et al.* Origin of the deep Bering Sea nitrate deficit: constraints from the nitrogen and oxygen isotopic composition of water column nitrate and benthic nitrate fluxes. *Glob Biogeochem Cycles* 2005;**19**:19. https://doi.org/10.1029/2005GB002508
17. Sigman DM, DiFiore PJ, Hain MP. *et al.* The dual isotopes of deep nitrate as a constraint on the cycle and budget of oceanic

fixed nitrogen. *Deep Sea Res 1 Oceanogr Res Pap* 2009;**56**:1419–39. https://doi.org/10.1016/j.dsr.2009.04.007
18. Casciotti KL, Buchwald C, McIlvin M. Implications of nitrate and nitrite isotopic measurements for the mechanisms of nitrogen cycling in the Peru oxygen deficient zone. *Deep Sea Res 1 Oceanogr Res Pap* 2013;**80**:78–93. https://doi.org/10.1016/j.dsr.2013.05.017
19. Buchwald C, Santoro AE, Stanley RHR. *et al.* Nitrogen cycling in the secondary nitrite maximum of the eastern tropical North Pacific off Costa Rica. *Glob Biogeochem Cycles* 2015;**29**:2061–81. https://doi.org/10.1002/2015GB005187
20. Peters BD, Babbin AR, Lettmann KA. *et al.* Vertical modeling of the nitrogen cycle in the eastern tropical South Pacific oxygen deficient zone using high-resolution concentration and isotope measurements. *Glob Biogeochem Cycles* 2016;**30**:1661–81. https://doi.org/10.1002/2016GB005415
21. Martin TS, Primeau F, Casciotti KL. Assessing marine nitrogen cycle rates and process sensitivities with a global 3-D inverse model. *Glob Biogeochem Cycles* 2019;**33**:1026–47. https://doi.org/10.1029/2018GB006088
22. Buchwald C, Casciotti K. Isotopic ratios of nitrite as tracers of the sources and age of oceanic nitrite. *Nat Geosci* 2013;**6**:1–6. https://doi.org/10.1038/ngeo1745
23. Brunner B, Contreras S, Lehmann MF. *et al.* Nitrogen isotope effects induced by anammox bacteria. *Proc Natl Acad Sci USA* 2013;**110**:18994–9. https://doi.org/10.1073/pnas.1310488110
24. Kobayashi K, Makabe A, Yano M. *et al.* Dual nitrogen and oxygen isotope fractionation during anaerobic ammonium oxidation by anammox bacteria. *ISME J* 2019;**13**:2426–36. https://doi.org/10.1038/s41396-019-0440-x
25. Kotajima S, Koba K, Ikeda D. *et al.* Nitrogen and oxygen isotope signatures of nitrogen compounds during anammox in the laboratory and a wastewater treatment plant. *Microbes Environ* 2020;**35**:n/a. https://doi.org/10.1264/jsme2.ME20031
26. Magyar PM, Hausherr D, Niederdorfer R. *et al.* Nitrogen isotope effects can be used to diagnose N transformations in wastewater anammox systems. *Sci Rep* 2021;**7850**. https://doi.org/10.1038/s41598-021-87184-0
27. Casciotti KL, McIlvin M, Buchwald C. Oxygen isotopic exchange and fractionation during bacterial ammonia oxidation. *Limnol Oceanogr* 2010;**55**:753–62. https://doi.org/10.4319/lo.2009.55.2.0753
28. Buchwald C, Casciotti KL. Oxygen isotopic fractionation and exchange during bacterial nitrite oxidation. *Limnol Oceanogr* 2010;**55**:1064–74. https://doi.org/10.4319/lo.2010.55.3.1064
29. Nishizawa M, Sakai S, Konno U. *et al.* Nitrogen and oxygen isotope effects of ammonia oxidation by thermophilic *Thaumarchaeota* from a geothermal water stream. *Appl Environ Microbiol* 2016;**82**:4492–504. https://doi.org/10.1128/AEM.00250-16
30. Buchwald C, Santoro AE, McIlvin MR. *et al.* Oxygen isotopic composition of nitrate and nitrite produced by nitrifying cocultures and natural marine assemblages. *Limnol Oceanogr* 2012;**57**:1361–75. https://doi.org/10.4319/lo.2012.57.5.1361
31. Boshers DS, Granger J, Tobias CR. *et al.* Constraining the oxygen isotopic composition of nitrate produced by nitrification. *Environ Sci Technol* 2019;**53**:1206–16. https://doi.org/10.1021/acs.est.8b03386
32. Kindaichi T, Awata T, Suzuki Y. *et al.* Enrichment using an upflow column reactor and community structure of marine anammox bacteria from coastal sediment. *Microbes Environ* 2011;**26**:67–73. https://doi.org/10.1264/jsme2.ME10158
33. Awata T, Oshiki M, Kindaichi T. *et al.* Physiological characterization of an anaerobic ammonium-oxidizing bacterium belonging to the '*Candidatus* Scalindua' group. *Appl Environ Microbiol* 2013;**79**:4145–8. https://doi.org/10.1128/AEM.00056-13
34. Ali M, Oshiki M, Awata T. *et al.* Physiological characterization of anaerobic ammonium oxidizing bacterium '*Candidatus* Jettenia caeni'. *Environ Microbiol* 2015;**17**:2172–89. https://doi.org/10.1111/1462-2920.12674
35. Oshiki M, Awata T, Kindaichi T. *et al.* Cultivation of planktonic anaerobic ammonium oxidation (Anammox) bacteria using membrane bioreactor. *Microbes Environ* 2013;**28**:436–43. https://doi.org/10.1264/jsme2.ME13077
36. Van De. *et al.* Autotrophic growth of anaerobic in a fluidized bed reactor. *Microbiology (N Y)* 1996;**142**:2187–96.
37. Strous M, Fuerst JA, Kramer EHM. *et al.* Missing lithotroph identified as new planctomycete. *Nature* 1999;**400**:446–9. https://doi.org/10.1038/22749
38. Casciotti KL, Böhlke JK, McIlvin MR. *et al.* Oxygen isotopes in nitrite: analysis, calibration, and equilibration. *Anal Chem* 2007;**79**:2427–36. https://doi.org/10.1021/ac061598h
39. Granger J, Sigman DM. Removal of nitrite with sulfamic acid for nitrate N and O isotope analysis with the denitrifier method. *Rapid Commun Mass Spectrom* 2009;**23**:3753–62. https://doi.org/10.1002/rcm.4307
40. APHA, AWWA, WEF. *Standard Methods for the Examination of Water and Wastewater*, 12th edn. Washington, D.C.: The American Public Health Association (APHA), American Water Works Association (AWWA), and Water Environment Federation (WEF), 2005.
41. Sigman DM, Altabet MA, Michener R. *et al.* Natural abundance-level measurements of the nitrogen isotopic composition of oceanic nitrate: an adaption of the ammonia diffusion method. *Mar Chem* 1997;**57**:227–42. https://doi.org/10.1016/S0304-4203(97)00009-1
42. Holmes RM, McClelland JW, Sigman DM. *et al.* Measuring $^{15}N\text{-}NH_4$ in marine, estuarine, and freshwaters: an adaptation of the ammonia diffusion method for samples with low ammonium concentrations. *MarChem* 1998;**60**:235–43. https://doi.org/10.1016/S0304-4203(97)00099-6
43. McIlvin MR, Altabet MA. Chemical conversion of nitrate and nitrite to nitrous oxide for nitrogen and oxygen isotopic analysis in freshwater and seawater. *Anal Chem* 2005;**77**:5589–95. https://doi.org/10.1021/ac050528s
44. Hu H, Bourbonnais A, Larkum J. *et al.* Nitrogen cycling in shallow low-oxygen coastal waters off Peru from nitrite and nitrate nitrogen and oxygen isotopes. *Biogeosciences* 2016;**13**:1453–68. https://doi.org/10.5194/bg-13-1453-2016
45. Kobayashi K. *et al.* Influence of $\delta^{18}O$ of water on measurements of $\delta^{18}O$ of nitrite and nitrate. *Rapid Commun Mass Spectrom* 2020;**35**:e8979. https://doi.org/10.1002/rcm.8979
46. Casciotti KL, Sigman DM, Hastings MG. *et al.* Measurement of the oxygen isotopic composition of nitrate seawater and freshwater using the dentirifier method. *Anal Chem* 2002;**74**:4905–12. https://doi.org/10.1021/ac020113w
47. Sigman DM, Casciotti KL, Andreani M. *et al.* A bacterial method for the nitrogen isotopic analysis of nitrate in seawater and freshwater. *Anal Chem* 2001;**73**:4145–53. https://doi.org/10.1021/ac010088e
48. Thuan NC, Koba K, Yano M. *et al.* N_2O production by denitrification in an urban river: evidence from isotopes, functional genes, and dissolved organic matter. *Limnology (Tokyo)* 2018;**19**:115–26. https://doi.org/10.1007/s10201-017-0524-0
49. McIlvin MR, Casciotti KL. Method for the analysis of $\delta^{18}O$ in water. *Anal Chem* 2006;**78**:2377–81. https://doi.org/10.1021/ac051838d

50. Granger J, Wankel SD. Isotopic overprinting of nitrification on denitrification as a ubiquitous and unifying feature of environmental nitrogen cycling. *Proc Natl Acad Sci USA* 2016;**113**:E6391–400. https://doi.org/10.1073/pnas.1601383113
51. Soetaert K, Petzoldt T. Inverse modelling, sensitivity and Monte Carlo analysis in R using package FME. *J Stat Softw* 2010;**33**:1–28. https://doi.org/10.18637/jss.v033.i03
52. Wunderlich A, Meckenstock RU, Einsiedl F. A mixture of nitrite-oxidizing and denitrifying microorganisms affects the $\delta^{18}O$ of dissolved nitrate during anaerobic microbial denitrification depending on the $\delta^{18}O$ of ambient water. *Geochim Cosmochim Acta* 2013;**119**:31–45. https://doi.org/10.1016/j.gca.2013.05.028
53. Zhang L, Okabe S. Ecological niche differentiation among anammox bacteria. *Water Res* 2020;**171**:115468. https://doi.org/10.1016/j.watres.2020.115468
54. Hu, Wessels HJCT, van Alen T. *et al.* Nitric oxide-dependent anaerobic ammonium oxidation. *Nat Commun* 2019;**10**:1244. https://doi.org/10.1038/s41467-019-09268-w
55. Kartal B, Kuypers MMM, Lavik G. *et al.* Anammox bacteria disguised as denitrifiers: nitrate reduction to dinitrogen gas via nitrite and ammonium. *Environ Microbiol* 2007;**9**:635–42. https://doi.org/10.1111/j.1462-2920.2006.01183.x
56. Oshiki M, Ishii S, Yoshida K. *et al.* Nitrate-dependent ferrous iron oxidation by anaerobic ammonium oxidation (anammox) bacteria. *Appl Environ Microbiol* 2013;**79**:4087–93. https://doi.org/10.1128/AEM.00743-13
57. Van Der Star WRL. *et al.* An intracellular pH gradient in the anammox bacterium *Kuenenia stuttgartiensis* as evaluated by ^{31}P NMR. *Appl Microbiol Biotechnol* 2010;**86**:311–7. https://doi.org/10.1007/s00253-009-2309-9
58. Friedman SH, Massefski W, Hollocher TC. Catalysis of intermolecular oxygen atom transfer by nitrite dehydrogenase of *Nitrobacter agilis*. *J Biol Chem* 1986;**261**:10538–43. https://doi.org/10.1016/S0021-9258(18)67418-6
59. Strous M, Pelletier E, Mangenot S. *et al.* Deciphering the evolution and metabolism of an anammox bacterium from a community genome. *Nature* 2006;**440**:790–4. https://doi.org/10.1038/nature04647
60. Rathnayake RMLD, Oshiki M, Ishii S. *et al.* Experimental evidence for in situ nitric oxide production in anaerobic ammonia-oxidizing bacterial granules. *Environ Sci Technol* 2018;**52**:5744–52. https://doi.org/10.1021/acs.est.8b00876
61. Hooper AKK, A B. O_2 and H_2O are each the source of one O in NO_2^- produced from NH_3 by *Nitrosomonas*: ^{15}N-NMR evidence. *FEBS Lett* 1983;**164**:236–40. https://doi.org/10.1016/0014-5793(83)80292-0
62. Oshiki M, Mizuto K, Kimura ZI. *et al.* Genetic diversity of marine anaerobic ammonium-oxidizing bacteria as revealed by genomic and proteomic analyses of '*Candidatus* Scalindua japonica'. *Environ Microbiol Rep* 2017;**9**:550–61. https://doi.org/10.1111/1758-2229.12586
63. Chicano TM, Dietrich L, de Almeida NM. *et al.* Structural and functional characterization of the intracellular filament-forming nitrite oxidoreductase multiprotein complex. *Nat Microbiol* 2021;**6**:1129–39. https://doi.org/10.1038/s41564-021-00934-8
64. Martin TS, Casciotti KL. Nitrogen and oxygen isotopic fractionation during microbial nitrite reduction. *Limnol Oceanogr* 2016;**61**:1134–43. https://doi.org/10.1002/lno.10278
65. Granger J, Sigman DM. Nitrogen and oxygen isotope fractionation during dissimilatory nitrate reduction by denitrifying bacteria. *Limnol Oceanogr* 2008;**53**:2533–45. https://doi.org/10.4319/lo.2008.53.6.2533
66. Kritee K, Sigman DM, Granger J. *et al.* Reduced isotope fractionation by denitrification under conditions relevant to the ocean. *Geochim Cosmochim Acta* 2012;**92**:243–59. https://doi.org/10.1016/j.gca.2012.05.020
67. Treibergs LA, Granger J. Enzyme level N and O isotope effects of assimilatory and dissimilatory nitrate reduction. *Limnol Oceanogr* 2017;**62**:272–88. https://doi.org/10.1002/lno.10393
68. Asamoto CK, Rempfert KR, Luu VH. *et al.* Enzyme-specific coupling of oxygen and nitrogen isotope fractionation of the Nap and Nar nitrate reductases. *Environ Sci Technol* 2021;**55**:5537–46. https://doi.org/10.1021/acs.est.0c07816
69. Frey C, Hietanen S, Jürgens K. *et al.* N and O isotope fractionation in nitrate during chemolithoautotrophic denitrification by *Sulfurimonas gotlandica*. *Environ Sci Technol* 2014;**48**:13229–37. https://doi.org/10.1021/es503456g
70. Li S, Luo Z, Wang S. *et al.* Denitrification fractionates N and O isotopes of nitrate following a ratio independent of carbon sources in freshwaters. *Environ Microbiol* 2023;**25**:2404–15. https://doi.org/10.1111/1462-2920.16468

The ISME Journal, 2025, **19(1)**, wraf115
https://doi.org/10.1093/ismejo/wraf115
Original Article